J. Chem. Sci. (2018) 130:54
https://doi.org/10.1007/s12039-018-1451-2

REGULAR ARTICLE

Mid-infrared quantum cascade laser spectroscopy probing of the kinetics of an atmospherically significant radical reaction, $CH_3O_2 + NO_2 + M \rightarrow CH_3O_2NO_2 + M$, in the gas phase

APARAJEO CHATTOPADHYAY*, MONOJ SAMANTA, KOUSHIK MONDAL and TAPAS CHAKRABORTY*

Department of Physical Chemistry, Indian Association for the Cultivation of Science, 2A Raja S C Mullick Road, Jadavpur, Kolkata, West Bengal 700 032, India
E-mail: pcac@iacs.res.in; pctc@iacs.res.in

MS received 25 December 2017; revised 2 March 2018; accepted 22 March 2018; published online 7 May 2018

Abstract. The kinetic parameters of an important atmospheric reaction, $CH_3O_2 + NO_2 + M \rightarrow CH_3O_2NO_2 + M$, have been recorded by monitoring directly the changes in concentrations of methylperoxy radicals (CH_3O_2) in the gas phase employing a new mid-infrared quantum cascade laser (QCL)-based apparatus. CH_3O_2 radicals in our apparatus have been generated by pulsed UV laser (266 nm) photolysis of CH_3I in a gaseous mixture with oxygen. The absorption band corresponding to the mid-infrared O-O stretching fundamental of the peroxy radical, within a narrow spectral range, 1070–1120 cm^{-1}, has been recorded by tuning the wavelength of the QCL operated in CW mode. The kinetics of the aforementioned reaction of CH_3O_2 with NO_2 has been followed by analyzing the changes of the infrared (QCL) decay profile of CH_3O_2 at 9.1 μm (1098.9 cm^{-1}) maintaining a pseudo first order reaction condition. We noticed that the rate constant of the reaction at 298 K varies in the range of (1.21–3.08) $\times 10^{-12}$ cm^3 $molecule^{-1}$ s^{-1} for changing the total pressure in the range of 75–730 mbar. The absorption cross-section of CH_3O_2 at the probe wavelength (1098.9 cm^{-1}), has been estimated for the first time to be $8.3 \pm 0.4 \times 10^{-20}$ cm^2.

Keywords. Quantum cascade laser; time-resolved mid-infrared spectroscopy; transient absorption; peroxy radicals; absorption cross-section.

1. Introduction

Investigation of the kinetics of gas phase radical reactions is important in many interrelated research fields like atmospheric chemistry, combustion chemistry, chemistry of interstellar medium to name but a few.[1–6] Detection of gas phase organic radicals is tricky because of their transient nature with a typical lifetime of a few microseconds to several minutes depending on the environment and nature of the radical. Therefore, time-resolved spectroscopic techniques are required for probing the gas phase transient radicals. Several time-resolved probing methods were developed over the last few decades and the most popular methods available in the literature are based on laser induced fluorescence (LIF) spectroscopy, UV/ Visible/ NIR absorption spectroscopy, mass spectrometry, etc.[7–16] Each of these probing techniques has its own merits as well as limitations. For example, laser induced fluorescence (LIF) is known to be an extremely sensitive method for detection of fluorescent radicals, but for non-fluorescent species, viz. organic peroxy radicals, the method cannot be used directly.[7,8,13,14] Likewise, in spite of being extremely sensitive, simple mass spectrometric technique cannot be used in differentiating isomeric species present in a gas mixture. Organic radicals usually have strong absorption bands in ultraviolet, and for that reason UV spectroscopy is being used extensively over a long period for probing different radical species.[9,17–19] However, an inherent problem of the method is that the UV absorption bands are usually broad, and in consequence it can have only limited use when more than one radical species are present in a gas mixture, which display overlapping absorption bands.[9,17]

In recent years, near-infrared (NIR) and visible spectroscopy, coupled with cavity enhanced methods, e.g., cavity ring down spectroscopy (CRDS) have emerged as powerful tools for probing the kinetics of organic radical reactions.[16,20,21] Although NIR spectroscopy provides better selectivity in comparison with the methods based

*For correspondence

on UV absorption, the small NIR absorption cross-sections of organic species is a serious disadvantage in kinetics measurements at low concentrations of the radical species. On the other hand, the characteristic vibrational bands of organic species, particularly in the mid-IR fingerprint region are very sharp with typically more than on order of magnitude absorption cross-section values, and the concerned species in a mixture can be selectively probed for measurement of reaction kinetics.[22–24] Therefore, the band selective mid-infrared spectroscopic method should be superior in studies of kinetics of the radical species produced by laser photolysis method, because typically more than one radical species are produced in more than one dissociation pathways. However, in the literature, the reports on mid-infrared (MIR) probing of organic radicals for kinetics measurements of fast radical reactions are rare, and this is mainly due to non-availability of stable commercial lasers in this optical region.[22,23] Recently, Quantum Cascade Lasers (QCLs) have been introduced as stable and intense laser sources in the MIR spectral region. We describe here a QCL-based methodology in reaction kinetics studies of gaseous radical species. The reaction used to demonstrate the potential of the method is the reaction (Eq. 1), where an adduct between methylperoxy radical (CH_3O_2) and nitrogen dioxide (NO_2) is produced *via* three body collision involving a background gas molecule (M = N_2, Ar, etc.).

$$CH_3O_2 + NO_2 + M \rightarrow CH_3O_2NO_2 + M \quad (1)$$

Methylperoxy radical is an important intermediate in the oxidation of volatile organic compounds (VOCs) in the atmosphere and also in combustion systems.[25–27] From the perspective of atmospheric chemistry, it is an important reaction intermediate, especially with respect to the reactions that occur in polluted environments, where NO_2 concentrations are high. Recently, this reaction (Eq. 1) has gained much attention, because, similar to much discussed peroxyacetylnitrate (PAN), peroxymethylnitrate ($CH_3O_2NO_2$) can also have a long lifetime, especially at upper troposphere, and thus the species can act as a sink as well as a transporting agent of NO_2.[28,29] It is important therefore to estimate the accurate kinetic data of the reaction of NO_2 with CH_3O_2 and other RO_2 species, because, atmospheric NO_2 concentration has a large effect on the tropospheric abundances of O_3 and OH radical. The lifetime of $CH_3O_2NO_2$ is highly sensitive to temperature, and it is less than a second at room temperature near sea level, but it could be as long as several days in the upper troposphere at low temperatures.[28,29] Recently, Nault *et al*., measured the concentration of $CH_3O_2NO_2$ in the upper troposphere by an aircraft campaign (~100 parts per trillion by volume (pptv) at higher altitudes and ~35 pptv at lower altitudes).[29] Thus, because of the enormous atmospheric significances, it is essential to have reliable experimental data concerning accurate values of the rate constants of this reaction in different conditions, and also to verify the rate constant data employing different probing methodologies. Although kinetics of this reaction has been studied before by several methods, we report here the measurement of the same by direct IR absorption monitoring of CH_3O_2 radical for the first time.[30–37] Recently, Lee and co-workers measured vibrational spectrum of various peroxy radicals in the mid-infrared by Step-Scan FTIR method at low spectral resolutions, but no kinetic data of those radicals were reported using this method.[38–40] We also have measured for the first time the infrared absorption cross-section of the peroxy radical near the band maximum of its O-O stretching fundamental.

2. Experimental

2.1 *Chemical reactor and gas handling system*

A schematic of the experimental setup is depicted in Figure 1.

The reactor is a cylindrical stainless steel tube of length 105 cm and inner diameter 2.5 cm. Two ends of the tube are closed with two CaF_2 windows and sealed by silicon gaskets. CaF_2 has high transmittance with respect to UV (266 nm), mid-IR (9–10 μm) and visible (532 nm) wavelengths, and thus the lasers are introduced into the cell through the windows. The gas inlet and outlet ports are placed at the two opposite ends of the reactor. The distance between these two ports along the length of the cell is ~100 cm. A separate mixing chamber of volume ~4 L has been used to prepare the reaction gas mixture. The gas mixture (CH_3I vapour diluted in N_2/O_2 mixture) is introduced into the reactor as a continuous flow through the sample inlet, and drained out through the outlet port by a root pump (Adixen ACP 15). The flow of the gas mixture is controlled by a precision metering valve (Swagelok) and the flow rate is monitored both at the inlet and outlet by two mechanical flow meters (Rota Yokogawa), and the mean of the two flow meters reading is typically ~5−25 L/min. A high pressure gauge (Pfeiffer CMR 361) is attached with a vacuum port located at the middle of the reactor. The temperature within the flow reactor remains almost the same as that of the room temperature (298 K), which has been measured using a thermocouple temperature sensor attached at one of the terminal ports.

2.2 *Optical system*

2.2a *Photolysis system*: For generation of radicals, the precursor compound (CH_3I in the present case), is photolyzed

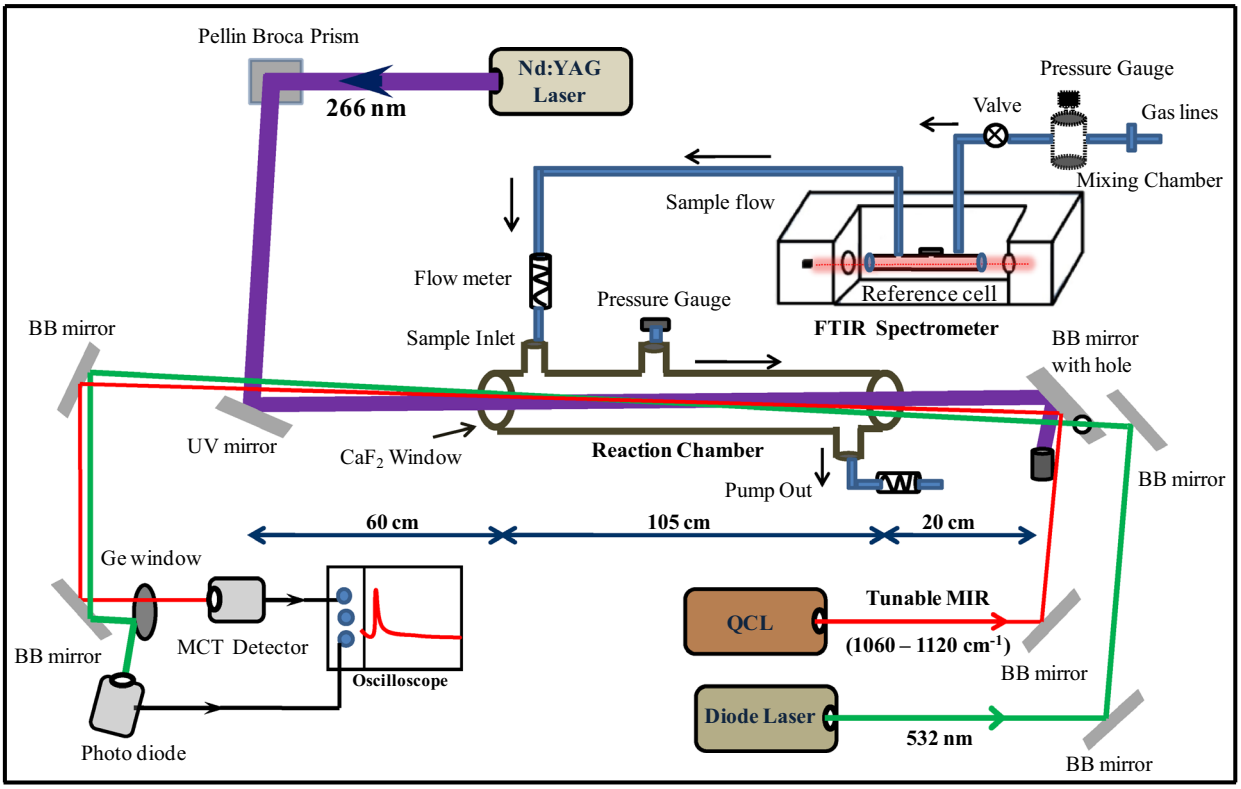

Figure 1. Schematic diagram of the pulsed laser photolysis time-resolved IR absorption kinetics measurement apparatus. Overall length of the reactor is 105 cm, and the distance between inlet and outlet ports of reaction gas mixture is 100 cm. Distance between UV mirror and input window of the reactor is 60 cm, while the same in the other side is 20 cm (distances mentioned in the figure are not scaled). The BB (broadband) mirror is coated with protected aluminum (450 nm−20 μm). UV and IR beams are aligned at ∼2° with respect to each other that results in 100 cm overlap between them within the reactor.

by the 4th harmonic UV light pulses (266 nm) of a Q-switched Nd:YAG laser (Spectra Physics Quanta-Ray Lab Series 150). The photolysis laser beam is introduced into the reactor through center of one of the terminal windows, and the beam passes through the reactor along its central axis. The beam shape of the photolysis laser is nearly circular with a diameter of 8 mm. The laser is operated at 10 Hz repetition rate, and typical pulse energy is ∼10 mJ.

2.2b *Probe laser*: The infrared beam from a QCL laser (Pranalytica Inc., Model: Omnilux), which was operated in continuous wave (CW) mode, is introduced into the reactor in counter propagating direction with respect to the photolysis laser keeping a small angle between the two beams so that they can have overlap within the reactor to the largest possible extent. The beam diameter of the IR laser is ∼2 mm while the same for the UV laser is ∼8 mm and this is particularly helpful in keeping the two lasers overlapped over a longer distance. The angle between the two laser beams is ∼2°, and for achieving this situation the input windows of the cell are kept far away from the folding mirrors that steer the beams into the reactor. The distance between the UV quartz mirror and starting point of the overlap between the two lasers is approximately 63 cm. This large distance results in the effective gap of ∼1 cm between the two laser beams near UV mirror. The QCL has a visible beam guide of HeNe laser, which is extremely helpful to monitor the alignment for beam overlap. At the exit end, the distance between the output window and the broad band (BB) IR mirror is nearly 20 cm. We have estimated that the overlap length between the two lasers within the cell is ∼100 cm, and this has been considered as the effective reaction path length for absorption of probe wavelength by the peroxy radicals. The range of frequency tunability of the QCL laser for this mode of operation is ∼60 cm^{-1} (wavelength maximum, 9.1 μm) and has a linewidth of ∼0.003 cm^{-1} with a power of ∼100 mW at the peak of the laser emission profile. The wavelength calibration of the QCL is verified by measuring the infrared fundamental band profile of acetone vapor (at room temperature) near 1091 cm^{-1} and a comparison of the recorded spectrum with the one recorded using a FTIR spectrometer is shown in Figure 2.

2.2c *Reactant concentration monitoring by optical methods*: Rate constants of bimolecular reactions are generally measured adopting pseudo first order conditions where one of the reactants is kept in excess compared to the other, and the same approach is adopted here for measuring the

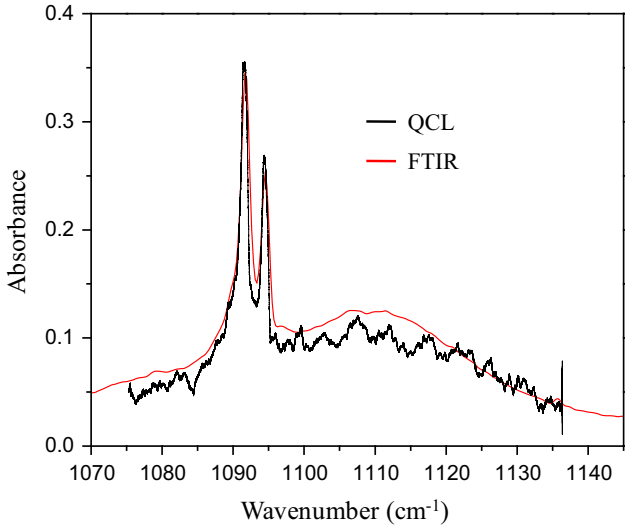

Figure 2. A comparison of the spectral features of the infrared 1091 cm^{-1} band of acetone vapor at room temperature recorded in transmission mode by continuous scanning of the QCL, with the spectrum obtained using a FTIR spectrometer (Model: IFS66S, Bruker Optics). For the latter, the spectrometer resolution is maintained at 0.25 cm^{-1}. The depicted comparison ensured the wavelength calibration of the QCL used.

rate constant of reaction in Eq. 1. For accurate measurement of the rate constant under this condition, precise measurements of the concentrations of the reactants within the reactor, particularly for NO_2 which is taken in excess is important and the following arrangement is made for this purpose. The reaction gas mixture is first flown through a reference cell placed directly inside the sample compartment of a FTIR spectrometer (Bruker IFS 66 s), and this arrangement enables monitoring absolute concentrations of the different reactants used. In addition, an *in situ* arrangement for NO_2 concentration monitoring has been made by introducing a CW beam of wavelength 532 nm from a diode laser which is aligned with the photolysis laser (Figure 1). The attenuation of 532 nm laser intensity was recorded continuously for monitoring the actual concentration of NO_2 inside the main reactor. Absorption cross-section of NO_2 at 532 nm is $\sigma = 1.50 \times 10^{-19}$ cm^2 $molecule^{-1}$.[41] Absolute concentrations of CH_3O_2 radicals are evaluated from time-resolved mid-IR absorption data. The required absorption cross-section value of the radical at 9.1 μm is also measured for the first time in the present study.

2.3 *Signal detection and data recording*

The intensity of the probe IR beam after exiting the reaction chamber is monitored by a fast pre-amplified MCT detector (VIGO PVMI-4TE-10.6). The time-resolved absorption signal from the detector is viewed, averaged and stored in a digital storage oscilloscope (Lecroy wavesurfer 62Xs, 600 MHz, 2.5 GS/s). A 50 Ω termination was used at the input of the oscilloscope. Typically, the decay signals were averaged over 50–100 laser pulses before recording. For further improvement of the signal to noise ratio (S/N), the data are treated with Savitzky-Golay smoothing algorithm.[42] This same smoothing algorithm was used in a previous study for measuring the kinetics of reaction (Eq. 1).[31] The output of 532 nm diode laser is detected by a photodiode and the signal is sent to the same oscilloscope for records. Since both the beams propagate through the cell along almost the same path, the latter is separated from the former by placing a Ge window in front of the MCT detector, which allows the IR beam to pass through but the wavelength 532 nm is reflected.

2.4 *Materials*

Methyliodide (CH_3I) was procured from Sigma Aldrich and used without further purification. The nitrogen and oxygen gases used were of the purity 99.99%. NO_2 was prepared by reaction of $NaNO_2$ with $FeSO_4.7H_2O$ in presence of excess oxygen, and the gas was dried by using a column of Na_2CO_3 before introducing into the mixing chamber.

3. Results and Discussion

3.1 *Measurement of the kinetics of* $CH_3O_2 + NO_2 + M \rightarrow CH_3O_2NO_2 + M$ *reaction*

3.1a *Production of* CH_3O_2 *radical*: In the presence of oxygen, methyl radical (CH_3) produced *via* photolysis of methyliodide (CH_3I) by 266 nm UV laser pulses of a Q-switched Nd:YAG laser (4^{th} harmonic wavelength), reacts to generate CH_3O_2 radical. At this wavelength, the absorption cross-section of CH_3I is very large ($\sigma \sim 1 \times 10^{-18}$ cm^2 $molecule^{-1}$), and photodissociation quantum yield (Φ) for production of CH_3 radical is effectively unity.[41,43,44] The concentration of the CH_3 radicals produced is determined in the following way:

$$\text{Methyl radical concentration, } [CH_3] = [CH_3I] \text{x } \sigma \text{ x} \Phi \text{x F} \quad (2)$$

where, $[CH_3I]$ is the concentration of the precursor CH_3I, σ the absorption cross-section of CH_3I at 266 nm, Φ the quantum yield of photo-dissociation of CH_3I at 266 nm, and F the laser fluence.

In the present experiment for kinetic measurements, concentration of CH_3I being $\sim 1 \times 10^{16} - 5 \times 10^{16}$ molecule cm^{-3} (determined from FTIR absorption data) and laser fluence $\sim 2 \times 10^{16}$ photons cm^{-2}, the estimated concentration of the produced CH_3 radical is typically $(2-10) \times 10^{14}$ cm^{-3}. Adduct formation of CH_3 radical with O_2 is a termolecular reaction (Eq. 3) and the following are the values of the rate constants:

$$CH_3 + O_2 + M \rightarrow CH_3O_2 + M. \quad (3)$$

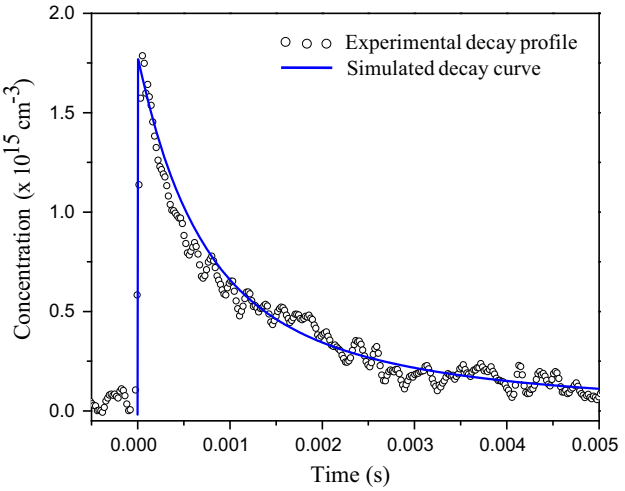

Figure 3. A typical decay signal of CH_3O_2 radicals (in the absence of NO_2) for probing at 9.1 μm. $[CH_3I] = 4.9 \times 10^{16}$ cm^{-3}, $[O_2] = \sim 9.0 \times 10^{17}$ cm^{-3} and total pressure of the reaction cell was 520 mbar. The decay curve obtained from modeling (blue trace) is also presented for a comparison with the experimental signal.

Here, $k_0 = 7.0 \times 10^{-31}$ $[N_2]$ cm^3 molecule^{-1} s^{-1} and $k_\infty = 1.8 \times 10^{-12}$ cm^{3}molecule^{-1} s^{-1}. k_0 and k_∞ are low and high pressure rate constants, respectively, at 298 K.[43,44] Almost all of CH_3 radicals produced by such means is converted into the peroxy radicals, CH_3O_2, within a few microseconds. Thus, at 520 mbar total pressure and in the absence of NO_2, it has been estimated from a reaction modeling study (described later) that the number of CH_3 radicals produced on average from each laser shot, 5.0×10^{14} cm^{-3}, is converted into CH_3O_2 with a number density of 4.7×10^{14} cm^{-3} within 10 μs. Depicted in Figure 3 is a typical decaying signal of CH_3O_2 radicals (in absence of NO_2) probed at 9.1 μm for a total pressure of 520 mbar. The detection limit of the methylperoxy radical in the current experimental setup is $\sim 2 \times 10^{14}$ cm^{-3}(S/N = 2). It should be noted that in Figure 3, the concentration of CH_3O_2 radical produced is much higher. However, for kinetic experiments, lower CH_3O_2 concentrations have been used.

As reported in previous studies, CH_3O_2 radicals could decay predominantly *via* the following self reaction pathways:[16,20,43–45]

$$CH_3O_2 + CH_3O_2 \rightarrow CH_3OH + HCHO + O_2, \quad k = 2.2 \times 10^{-13} \text{cm}^3 \text{ molecule}^{-1} \text{ s}^{-1} \quad (4a)$$

$$\rightarrow CH_3O + CH_3O + O_2, \quad k = 1.3 \times 10^{-13} \text{cm}^3 \text{ molecule}^{-1} \text{ s}^{-1} \quad (4b)$$

The following reactions also contribute to the decay of CH_3O_2 radicals.[43,44,46]

$$CH_3O_2 + CH_3 \rightarrow CH_3O + CH_3O, \quad k = 9.1 \times 10^{-11} \text{ cm}^3 \text{ molecule}^{-1} \text{ s}^{-1} \quad (5)$$

$$CH_3O + O_2 \rightarrow HCHO + HO_2, \quad k = 1.9 \times 10^{-15} \text{cm}^3 \text{ molecule}^{-1} \text{s}^{-1} \quad (6)$$

$$CH_3O_2 + HO_2 \rightarrow CH_3OOH + O_2, \quad k = 4.68 \times 10^{-12} \text{cm}^3 \text{ molecule}^{-1} \text{s}^{-1} \quad (7a)$$

$$\rightarrow HCHO + H_2O + O_2, \quad k = 5.20 \times 10^{-13} \text{cm}^3 \text{ molecule}^{-1} \text{s}^{-1} \quad (7b)$$

The production and decay of CH_3O_2 radicals as obtained from simulation considering reactions 3–7 is also presented in Figure 3 (blue trace), and this has been done using a standard computer program called ACUCHEM.[47] The experimental CH_3O_2 concentration profile shows satisfactory agreement with the modeled one. The fate of I atoms formed in the photolysis of CH_3I is as follows. I atoms rapidly combine with CH_3O_2 to form CH_3O_2I, which react very rapidly with I atoms to give rise to CH_3O_2 and I_2. As a result, there is practically no loss of CH_3O_2 radicals in this process.[20,48,49] It is worth mentioning here that the concentrations of the reactants used in our experiments are not too small, and when the reaction with these concentrations is performed in a static cell, we observe accumulation of molecular iodine (I_2) on the walls of the reactor. However, in the flowing reactor, with the flow rates that are typically used, we never noticed I_2 accumulation.

3.2 *Mid-IR absorption spectrum and absorption cross-section of CH_3O_2 radical*

The mid-infrared spectrum of CH_3O_2 radical has been measured previously by Huang *et al.*, using a step-scan FTIR method at a low spectral resolution of 4 cm^{-1}.[38] Using the QCL we have recorded the O-O stretching absorption profile of the radical within 1070–1120 cm^{-1} range with a laser resolution of 100 MHz by the following approach. Time-resolved absorption signals were recorded at discrete wavelengths (maintaining a step size of 1.5 cm^{-1}) operating the laser in CW mode. Absorbance value at each wavelength is measured using the standard relation, Absorbance (O.D.) = ln (I_0/I), where I_0 is the signal level before introducing photolysis laser and I, the signal after ~10 μs of firing of the photolysis laser. The spectrum, as shown in Figure 4, has been developed by line joining the discrete absorbance values as a function of laser frequency, and within the depicted spectral range it looks nearly similar to the one reported by Huang *et al.*[38] The segment of the band profile within 1070−1120 cm^{-1} range was assigned to a vibrational

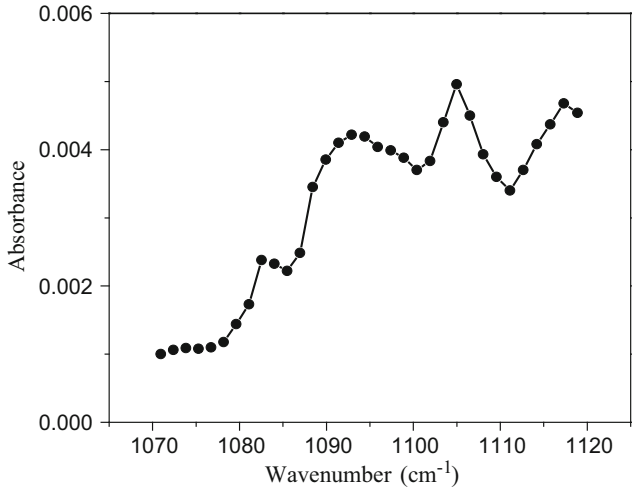

Figure 4. The infrared absorption spectrum of CH_3O_2 radical in the depicted spectral range permitted by the tunability of QCL. The detailed method used to record the spectrum has been discussed in the text.

fundamental corresponding to O-O stretch with a contribution from CH_3 rocking, and this band was shown to have a maximum at 1117 cm^{-1}. The same peak is also present in the spectrum shown in Figure 4, although the power of QCL is low at this wavelength. There is another peak at ~1094 cm^{-1}, and although no assignment for it was discussed in reference 38, on the basis of theoretical prediction it can be assigned to CH_3 wagging fundamental of the radical[38]. In measuring the decay kinetics, the radical has been probed at the maximum of the laser emission wavelength, 9.1 μm (1098.9 cm^{-1}), and it is seen that the radical has a considerably large absorbance at this wavelength, which results in a good signal-to-noise ratio.

The absorption cross-section (σ) at the probe wavelength has been evaluated in the following manner. The cross-section (σ) is defined as, σ = Absorbance/(n l), n denotes the concentration of CH_3O_2 radical and l, the optical path length. Here, absorbance is determined from the time-resolved absorption signal in the way mentioned before. Optical path length l is 100 cm. Precise measurement of n, i.e., the concentration of CH_3O_2 radical is important for accurate measurement of the cross-section (σ). A course measurement of the concentration of CH_3O_2 radical, i.e., n, is evaluated from laser fluence and CH_3I concentration following the procedure as mentioned previously. For fine measurement of the initial CH_3O_2 concentration, following approach has been taken. Recently, Farago *et al.,* measured the absorption cross-section of CH_3O_2radical at NIR region using a reaction model to accurately quantify the initial radical concentration and its time evolution.[20] The same approach has also been adopted previously by Pushkarsky *et al.,* and Atkinson *et al*.[16,45] In the present study, as shown in Figure 3, a simulation of the decay profile (considering reactions, Eqs. 3–7) of CH_3O_2 radicals is carried out. During the construction of the decay profile, the initial CH_3O_2 concentration is iterated so as to match the simulated decay profile well with the experimental plot as depicted in Figure 3. This initial CH_3O_2 concentration (1.8×10^{15} molecule cm^{-3}) is then used to estimate the absorption cross-section. Using this concentration data, the absorption cross-section of CH_3O_2 radical at 9.1 μm (1098.9 cm^{-1}) has been estimated to be 8.3×10^{-20} cm^2. Another source of uncertainty to the value of σ may come from the consideration of the effective optical path length as 100 cm which may typically vary within 5%. Considering this uncertainty, the value of absorption cross-section σ is taken as $8.3 \pm 0.4 \times 10^{-20}$ cm^2.

3.3 *Kinetics of $CH_3O_2 + NO_2$ reaction*

In presence of NO_2, CH_3O_2 reacts with NO_2 (Eq. 1) apart from the self reactions. The kinetics experiments were performed under pseudo-first order condition where $[NO_2] > [CH_3O_2]$.

Before presenting our results, first we review here the studies performed earlier. In the decade of 1980 s, four different research groups carried out measurements independently by probing CH_3O_2 radical at an ultraviolet wavelength near 250 nm.[30–33] Using the same method, Bridier *et al.,* studied the reaction in the temperature range of 333–373 K at 730 Torr pressure, and Wallington *et al*., measured the rate constant values in the pressure range of 0.5–14 atm at 295 K.[34,35] As pointed out before, although the UV absorption cross-section is higher, but UV absorption band is very broad and that limits selectivity. Later, Bacak *et al.,* used chemical ionization mass spectrometry as a probe to study the reaction at low temperatures.[36] Very recently, McKee *et al*., studied the kinetics of the reaction as well as equilibrium parameters for the process $CH_3O_2 + NO_2 \leftrightarrow CH_3O_2NO_2$ by probing CH_3O_2 radicals indirectly.[37] CH_3O_2 was photolyzed to produce CH_3O and OH radicals, and these secondary radicals were probed by laser induced fluorescence spectroscopic method.

Figure 5 represents a typical decay profile for IR absorption of CH_3O_2 radical at the probing wavelength (9.1 μm) in presence of NO_2 under the condition of a fast flow of the reaction gas mixture within the reactor. An important merit of the method, in spite of smaller infrared absorption cross-section of the radical at this wavelength in comparison with the previously used UV probing wavelength, is that in the absence of photolysis laser the background absorption of the gas mixture is

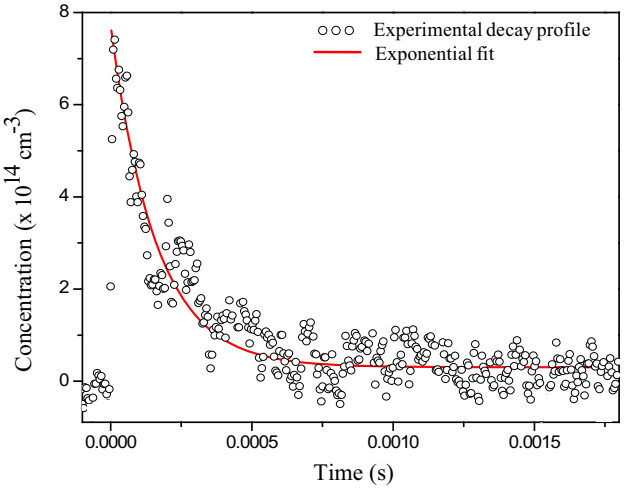

Figure 5. Decaying IR absorption signal of CH_3O_2 radicals in presence of NO_2 at 75 mbar total pressure. The initial concentration of CH_3O_2 radical and NO_2 are 7.30×10^{14} cm^{-3} and 5.30×10^{15} cm^{-3}, respectively. It is seen that the decay can be nicely fitted with a single exponential decay curve.

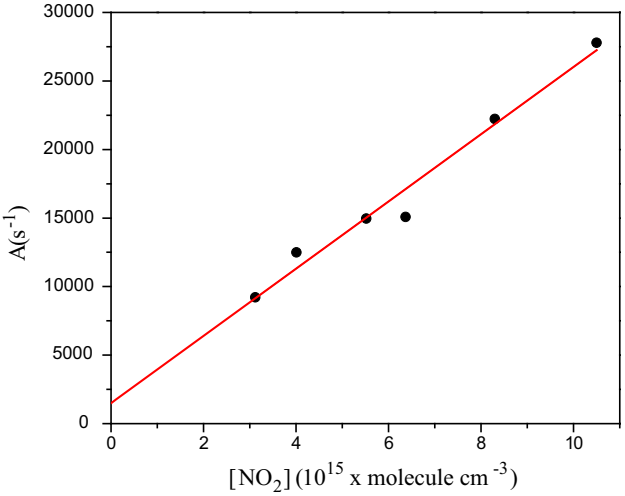

Figure 6. Plot depicting the changes of the estimated values of the decay constant (A) for different concentrations of NO_2 (total pressure 305 mbar).

zero and the adduct formed $CH_3O_2NO_2$ also does not absorb at this wavelength.[50]

It is notable that for maintaining pseudo first order reaction conditions the concentration ratio, $[NO_2]$: $[CH_3O_2]$, has been varied within the range of ~8—40. Although this ratio is relatively small, but the single exponential behavior of the plot in Figure 5 indicates that the pseudo first order condition is indeed achieved around this value of the concentration ratio. At still higher concentrations of NO_2we have noticed occurrence of dimer (N_2O_4) formation (N_2O_4 was probed at 750 cm^{-1} by FTIR). Since the reaction rate of N_2O_4 with $CH_3O_2$is not known, to avoid possible source of errors for such dimer formation, NO_2 concentration was kept below $\sim 1 \times 10^{16}$ cm^{-3}, and no prominent sign of dimer formation was observed at this concentration of NO_2. We would like to point out here that in a number of previous studies, pseudo first order condition was invoked upon use of the same concentration ratio between NO_2 and CH_3O_2.[30,31] In addition, the linear plot of variation of the decay constant with $[NO_2]$ in the reactor as depicted in Figure 6 (discussed below) is a direct support in favor of pseudo 1st order behavior of the reaction. The rate constant of the reaction (Eq. 1) has been measured in the following way.

The associated time constant (τ) for decay of the individual CH_3O_2 absorption trace is measured by fitting the decay curve with an exponential function as stated earlier. The decay rate constant (A) is the reciprocal of the corresponding time constant ($A = 1/\tau$). The reaction rate constant (k) is calculated from decay constant A using the following relation:

$$A = k_1 + A_d = k[NO_2] + A_d \quad (8)$$

where, A = decay constant, k_1 = pseudo first order rate constant, k = bimolecular rate constant, $[NO_2]$ = concentration of NO_2 (molecule cm^{-3}), A_d = decay constant of CH_3O_2 in the absence of NO_2. The slope of the plot of A vs $[NO_2]$ gives the bimolecular rate constant for the reaction. A representative plot of the decay constant (A) vs concentration of NO_2 is presented in Figure 6. The experiment has been performed in N_2 buffer gas with a total pressure of 305 mbar. The slope of the linear plot, i.e. the rate constant of the reaction is $k = 2.45 \pm 0.47 \times 10^{-12}$ cm^3 $molecule^{-1}$ s^{-1} (error limit: 2σ).

It is worth mentioning about a possible error source concerning depletion in concentration of NO_2 as a result of UV photolysis. The UV absorption cross-section of NO_2 at 266 nm is typically low, $\sim 2.2 \times 10^{-20}$ cm^2, and although the quantum yield for photodissociation of NO_2 at this wavelength is not known, but for the sake of discussion we have considered it to be 1. For NO_2 concentration of 5.30×10^{15} cm^{-3} (Figure 5), the extent of its loss for each laser pulse has been calculated (following Eq. 2) and the value is 4.10×10^{12} cm^{-3}, which is quite low. Moreover, the actual concentration of NO_2 inside the reactor during the laser photolysis is probed by a 532 nm CW diode laser, and the change of its signal in the presence and absence of the photolysis laser is also not significant.

3.4 *Effect of total pressure on rate constant*

The reaction was studied at different total pressures within the range of 75–730 mbar at 298 K by varying

Table 1. Bimolecular rate constant values estimated as a function of total pressure using N_2 as the buffer gas (error is 2σ).

Pressure (mbar)	Bimolecular rate constant k (10^{-12}cm^3 molecule^{-1} s^{-1})
730	3.08 ± 0.36
545	2.75 ± 0.30
305	2.45 ± 0.47
255	2.19 ± 0.39
75	1.21 ± 0.27

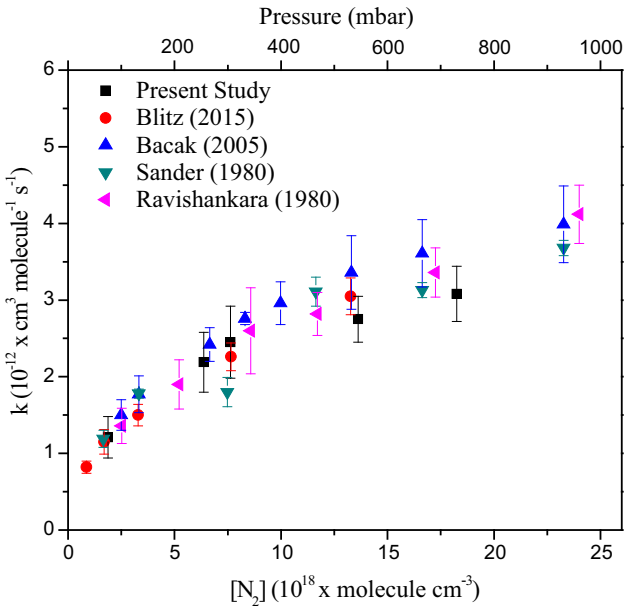

Figure 7. Plot depicting the variation of the rate constant for reaction between NO_2 and CH_3O_2 due to change in N_2 buffer gas pressure. The observed results [■] are compared with similar studies performed earlier.

the partial pressure of N_2 buffer gas, and the rate constant values estimated are shown in Figure 7 as well as in Table 1. As expected for an adduct formation reaction, the rate constant decreases steadily with decrease in total pressure.

In Figure 7, a comparison of the changes of the estimated values of the rate constants with total pressure in the present study with those reported by other workers by use of different methods is shown. It is seen that the agreements are very much satisfactory in lower pressure range. At higher pressures, although the rate constant values estimated here by direct infrared probing of CH_3O_2 radical is a little smaller compared to the UV absorption probing, the values fall within the error range.

4. Conclusions

We have demonstrated here that a quantum cascade laser-based time-resolved mid-infrared absorption spectroscopic method can be used as an effective means for measuring the kinetic parameters of radical reactions in the gas phase. The performance of the apparatus has been demonstrated measuring the reaction kinetics of a tropospherically important reaction between CH_3O_2 radical and NO_2. Our estimated rate constant of the reaction for the range of total pressure between 75 and 730 mbar varies between $(1.21-3.08) \times 10^{-12}$ cm^3 molecule^{-1} s^{-1} which agree quite satisfactorily with the previous reports. The major merit of the method, in comparison to much used UV probing of the radicals, is selectivity with respect to specific reactant or product of the reaction, and this is possible due to narrower spectral widths of the infrared bands in comparison with typically broad UV spectral bands. On the other hand, larger absorption cross-sections of the UV bands of the radicals in comparison with mid-infrared bands, and also easy availability of intense and narrow bandwidth UV light source are the primary factors for the popularity of the UV-based spectroscopic methods. We would also like to make a remark that for having only a single pass of optical path (path length ~100 cm), the detection sensitivity of this apparatus appears smaller compared to other much used methods, e.g. cavity ring down spectroscopy (CRDS), and partly also due to relatively lower absorption cross-sections of radicals in mid-IR spectral range. For methylperoxy radical, the detection limit of our apparatus has been shown to be $\sim 2 \times 10^{14}$ cm^{-3}. On the other hand, typical optical path length for cavity ring down spectroscopy (CRDS) is ~1 km, which results in detection limit of $\sim 10^{11}-10^{12}$ cm^{-3}. The laser induced fluorescence (LIF) or mass spectrometric techniques also have similar detection limit. In near future, we plan to replace the linear reactor by a Herriott type multi-pass absorption cell, which will enable us in detecting the peroxy radicals with concentration as low as $\sim 5 \times 10^{12}$ cm^{-3}. Furthermore, we intend to investigate the reactions of NO and NO_2 with other atmospherically important peroxy radicals.

Acknowledgements

The authors sincerely acknowledge the financial support received from the Department of Science and Technology, Govt. of India, under the Scheme Number SB/S1/PC-027/2013. AC thanks CSIR, Govt. of India and IACS for the Senior Research Fellowship, MS and KM thank UGC, Govt. of India for Junior Research Fellowships.

References

1. Cox R A 2003 Chemical Kinetics and Atmospheric Chemistry: Role of Data Evaluation *Chem. Rev.* **103** 4533
2. Jacob D J 1999 Introduction to Atmospheric Chemistry (Princeton University Press: Princeton) p. 157
3. Orlando J J and Tyndall G S 2012 Laboratory studies of organic peroxy radical chemistry: an overview with emphasis on recent issues of atmospheric significance *Chem. Soc. Rev.* **41** 6294
4. Miller J A, Kee R J and Westbrook C K 1990 Chemical kinetics and combustion modeling *Annu. Rev. Phys. Chem.* **41** 345
5. Westbrook C K 2000 Chemical kinetics of hydrocarbon ignition in practical combustion systems *Proc. Combust. Inst.* **28** 1563
6. Smith I W M and Rowe B R 2000 Reaction Kinetics at Very Low Temperatures: Laboratory Studies and Interstellar Chemistry *Acc. Chem. Res.* **33** 261
7. Miller T A 2006 Spectroscopic probing and diagnostic of the geometric structure of the alkoxy and alkyl peroxy radical intermediates *Mol. Phys.* **104** 2581
8. Deng W, Wang C, Katz D R, Gawinski G R, Davis A J and Dibble T S 2000 Direct kinetic studies of the reactions of 2-butoxy radicals with NO and O_2 *Chem. Phys. Lett.* **330** 541
9. Lightfoot P D, Cox R A, Crowley J N, Destriau M, Hayman G D, Jenkin M E, Moortgat G K and Zabel F 1992 Organic peroxy radicals: Kinetics, spectroscopy and tropospheric chemistry *Atmos. Environ.* **26** 1805
10. Krasnoperov L N, Chesnokov E N, Stark H and Ravishankara A R 2005 Elementary reactions of formyl (HCO) radical studies by laser photolysis-transient absorption spectroscopy *Proc. Combust. Inst.* **30** 935
11. Raventós-Duran M T, Mcgillen M, Percival C J, Hamer P D and Shallcross D E 2007 Kinetics of the CH_3O_2 + HO_2 reaction: A temperature and pressure dependence study using chemical ionization mass spectrometry *Int. J. Chem. Kinet.* **39** 571
12. Elg A -P, Andersson M and Rosen A 1997 REMPI as a tool for studies of OH radicals in catalytic reactions *Appl. Phys. B* **64** 573
13. Rajakumar B, Portmann R W, Burkholder J B and Ravishankara A R 2006 Rate Coefficients for the Reactions of OH with $CF_3CH_2CH_3$ (HFC-263fb), CF_3CHFCH_2F (HFC-245eb), and $CHF_2CHFCHF_2$ (HFC-245ea) between 238 and 375 K *J. Phys. Chem. A* **110** 6724
14. Chai J, Hu H, Dibble T S, Tyndall G S and Orlando J J 2014 Rate Constants and Kinetic Isotope Effects for Methoxy Radical Reacting with NO_2 and O_2 *J. Phys. Chem. A* **118** 3552
15. Osborn D L, Zou P, Johnsen H, Hayden C C, Taatjes C A, Knyazev V D, North S W, Peterka D S, Ahmed M and Leone S R 2008 The multiplexed chemical kinetic photoionization mass spectrometer: A new approach to isomer-resolved chemical kinetics *Rev. Sci. Instrum.* **79** 104103
16. Atkinson D B and Spillman J L 2002 Alkyl Peroxy Radical Kinetics Measured Using Near-infrared CW-CavityRing Down Spectrometer *J. Phys. Chem. A* **106** 8891
17. Wallington T J, Dagaut P and Kurylo M J 1992 UV absorption cross sections and reaction kinetics and mechanisms for peroxy radicals in the gas phase *Chem. Rev.* **92** 667
18. Krasnoperov L N and Mehta K 1999 Kinetic Study of CH_3 + HBr and CH_3 + Br Reactions by Laser Photolysis – Transient Absorption over 1-100 Bar Pressure Range *J. Phys. Chem. A* **103** 8008
19. Krasnoperov L N, Chesnokov E N, Stark H and Ravishankara A R 2004 Unimolecular dissociation of formyl radical, $HCO \rightarrow H + CO$, studied over 1 – 100 bar pressure range *J. Phys. Chem. A* **108** 11526
20. Faragó E P, Viskolcz B, Schoemaecker C and Fittschen C 2013 Absorption Spectrum and Absolute Absorption Cross Sections of CH_3O_2 Radicals and CH_3I Molecules in the Wavelength Range $7473 - 7497\ cm^{-1}$ *J. Phys. Chem. A* **117** 12802
21. Rajakumar B, Gericzak T, Flad J E, Ravishankara A R and Burkholder J B 2007 Visible Absorption Spectrum of the CH_3CO Radical *J. Phys. Chem. A* **111** 8950
22. Miyano S and Tonokura K 2011 Measurements of nitrogen-broadening coefficients in the υ_3 band of the hydroperoxyl radical using a continuous wave quantum cascade laser *J. Mol. Spectrosc.* **265** 47
23. Sakamoto Y and Tonokura K 2012 Measurements of the Absorption Line Strength of Hydroperoxyl Radical in the υ_3 Band using a Continuous Wave Quantum Cascade Laser *J. Phys. Chem. A* **116** 215
24. Mah D A, Cabrera J, Nation H, Ramos M, Sharma S and Nickolaisen S L 2003 Mid-infrared Spectrum of the Gas Phase Ethyl Peroxy Radical: C_2H_5OO *J. Phys. Chem. A* **107** 4354
25. Salisbury G, Rickard A R, Monks P S, Allan B J, Bauguitte S, Penkett S A, Carslaw N, Lewis A C, Creasey D J, Heard D E, Jacobs P J and Lee J D 2001 Production of peroxy radicals at night via reactions of ozone and the nitrate radical in the marine boundary layer *J. Geophys. Res. [Atmos].* **106** 12669
26. Tyndall G S, Cox R A, Granier C, Lesclaux R, Moortgat G K, Pilling M J Ravishankara A R and Wallington T J 2001 Atmospheric chemistry of small organic peroxy radicals *J. Geophys. Res. [Atmos].* **106** 12157
27. Wang S, Miller D L, Cernansky N P, Curran H J, Pitz W J and Westbrook C K 1999 A flow reactor study of neopentane oxidation at 8 atmospheres: experiments and modeling *Combust. Flame* **118** 415
28. Murphy J G, Thornton J A, Wooldridge P J, Day D A, Rosen R S, Cantrell C, Shetter R E, Lefer B and Cohen R C 2004 Measurements of the sum of HO_2NO_2 and $CH_3O_2NO_2$ in the remote troposphere *Atmos. Chem. Phys.* **4** 377
29. Nault B A, Garland C, Pusede S E, Wooldridge P J, Ullmann K, Hall S R and Cohen R C 2015 Measurements of $CH_3O_2NO_2$ in the upper trosphere *Atmos. Meas. Tech.* **8** 987
30. Ravishankara A R, Eisele F L and Wine P H 1980 Pulsed laser photolysis-long path laser absorption kinetics study of the reaction of methylperoxy radicals with NO_2 *J. Chem. Phys.* **73** 3743
31. Sander S P and Watson R T 1980 Kinetics studies of the reactions of methylperoxy with nitric oxide, nitrogen

dioxide, and methyldioxy at 298 K *J. Phys. Chem.* **84** 1664
32. Adachi H and Basco N 1980 The reaction of CH_3O_2 radicals with NO_2 *Int. J. Chem. Kinet.* **XII** 1
33. Cox R A and Tyndall G S 1980 Rate Constants for the reactions of CH_3O_2 with HO_2, NO and NO_2 using Molecular Modulation Spectrometry *J.C.S. Faraday II* **76** 153
34. Bridier I, Lesclaux R and Veyret B 1992 Flash potolysis kinetic study of the equilibrium $CH_3O_2 + NO_2 = CH_3O_2NO_2$ *Chem. Phys. Lett.* **191** 259
35. Wallington T J, Nielsen O J and Sehested K Kinetics of the reaction of CH_3O_2 radicals with NO_2 1999 *Chem. Phys. Lett.* **313** 456
36. Bacak A, Bardwell M W, Ravento's-Duran M T, Percival C J, Hamer P D and Shallcross D E 2006 Kinetics of the $CH_3O_2 + NO_2$ reaction: A temperature and pressure dependence study using chemical ionistion mass spectrometry *Chem. Phys. Lett.* **419** 125
37. McKee K, Blitz M A and Pilling M J 2016 Temperature and Pressure Studies of The Reactions of CH_3O_2, HO_2 and 1,2-$C_4H_9O_2$ with NO_2 *J. Phys. Chem. A* **120** 1408
38. Huang D-R, Chu L-K and Lee Y-P 2007 Infrared absorption of gaseous CH_3OO detected with a step-scan Fourier-transform spectrometer *J. Chem. Phys.* **127** 234318
39. Chu L-K and Lee Y-P 2009 Infrared absorption of gaseous c-ClCOOH and t-ClCOOH recorded with a step-scan Fourier-transform spectrometer *J. Chem. Phys.* **130** 174304
40. Chu L-K and Lee Y-P 2010 Transient infrared spectra of CH_3SOO and CH_3SO observed with a step-scan Fourier-transform spectrometer *J. Chem. Phys.* **133** 184303
41. Keller-Rudek H, Moortgat G K, Sander R and Sörensen R 2013 The MPI-Mainz UV/VIS Spectral atlas of gaseous molecules of atmospheric interest *Earth Syst. Sci. Data* **5** 365
42. Savitsky A and Golay M J E 1964 Smoothing and differentiation of data by simplified least squares procedures *Anal. Chem.* **36** 1627
43. Atkinson R, Baulch D L, Cox R A, Crowley J N, Hampson R F, Hynes R G, Jenkin M E, Rossi M J and Troe J 2006 Evaluated kinetic and photochemical data for atmospheric chemistry: Volume II-gas phase reactions of organic species *Atmos. Chem. Phys.* **6** 3625. IUPAC Subcommittee for Gas Kinetic Data Evaluation, (http://iupac.pole-ether.fr) (Accessed on 1 March 2018)
44. Atkinson R, Baulch D L, Cox R A, Crowley J N, Hampson R F, Hynes R G, Jenkin M E, Rossi M J and Troe J 2004 Evaluated kinetic and photochemical data for atmospheric chemistry: Volume I-gas phase reactions of O_x, HO_x, NO_x and SO_x species *Atmos. Chem. Phys.* **4** 1461. IUPAC Subcommittee for Gas Kinetic Data Evaluation, (http://iupac.pole-ether.fr) (Accessed on 1 March 2018)
45. Pushkarsky M B, Zalyubovsky S J and Miller T A 2000 Detection and characterization of alkyl peroxy radicals using cavity ring down spectroscopy *J. Chem. Phys.* **112** 10695
46. Keiffer M, Miscampbell A J and Pilling M J 1988 A global technique for analyzing multiple decay curves. Application to the $CH_3 + O_2$ system *J. Chem. Soc. Faraday Trans.* **84** 505
47. Braun W, Herron J T and Kahaner D K 1988 Acuchem: A computer program for modeling complex chemical reaction systems *Int. J. Chem. Kinet.* **20** 51
48. Jenkin M E and Cox R A 1991 Kinetics of reactions of CH_3O_2 and $HOCH_2CH_2O_2$ radicals produced by the photolysis of iodomethane and 2-iodoethanol *J. Phys. Chem.* **95** 3229
49. Dillon T J, Tucceri M E and Crowley J N 2006 Laser induced fluorescence studies of iodine oxide chemistry part II. The reactions of IO with CH_3O_2, CF_3O_2 and O_3. *Phys. Chem. Chem. Phys.* **8** 5185
50. Niki H, Maker P D, Savage C M and Breitenbach L P 1978 FTIR spectroscopic observation of peroxymethyl nitrate formed via ROO + NO_2 → $ROONO_2$ *Chem. Phys. Lett.* **55** 289